

Effect of vacuum scheme on radiative sky cooling performance

Mingke Hu ^a, Bin Zhao ^b, Suhendri ^a, Jingyu Cao ^c, Qiliang Wang ^d, Saffa Riffat ^a, Yuehong Su ^{a, *}, Gang Pei

^{b, *}

^a *Department of Architecture and Built Environment, University of Nottingham, University Park, Nottingham NG7 2RD, UK*

^b *Department of Thermal Science and Energy Engineering, University of Science and Technology of China, Hefei 230027, China*

^c *College of Civil Engineering, Hunan University, Changsha 410082, China*

^d *Department of Building Services Engineering, The Hong Kong Polytechnic University, Kowloon, Hong Kong, China*

* Corresponding author: yuehong.su@nottingham.ac.uk; peigang@ustc.edu.cn

Abstract

Relatively low cooling power density is one of the main barriers to wider promotion of radiative sky cooling (RSC) technology. Vacuum scheme has been proposed to minimize the non-radiative cooling loss and thus improve the cooling capacity. However, systematic research to elucidate the effect of the vacuum mechanism on the RSC performance is still lacking. Therefore, in the present study, an RSC module with four vacuum structures is proposed to evaluate the performance variation resulting from the vacuum scheme. A quasi-steady state mathematical model is developed to characterize the cooling performance of the four RSC modules under different operation conditions. Results suggested that the vacuum strategy can further elevate the cooling capacity if the typical RSC (TRSC) module itself can realize all-day sub-ambient cooling. However, if the TRSC cannot achieve sub-ambient cooling during peak sun hours, the vacuum scheme will deteriorate rather than ameliorate the cooling performance. On a typical summer day in Shanghai, vacuumization in both cavities enables a further temperature reduction of 10.21 °C during the nighttime, but this value decreases to only 3.39 °C during the daytime. The cooling power enhancement resulting from the

vacuum scheme is limited in real-world dynamic operation with the thermal carrier. At a reasonable temperature gap of 5 °C between the emitter and ambient air, the extra cooling gain is less than 5.10 W/m². Hence, considering the addition of energy consumption and system complexity caused by the vacuum unit, it may not be advisable to pursue better cooling performance of a stand-alone RSC collector/system through introducing a vacuum strategy, unless realizing a deep stagnation emitter temperature is targeted.

Keywords: *radiative cooling; vacuum; stagnation temperature; cooling power.*

1. Introduction

Radiative sky cooling (RSC) is a completely passive and renewable cooling scheme which takes the frigid outer space as the heat sink [1-3]. The well-known transparent “atmospheric window” lying in 8–13 μm allows a terrestrial object to radiatively dump heat into the deep universe and cool itself down to a sub-ambient temperature in most cases [4, 5]. That means, if the emitter is highly sunlight-rejected and well thermal insulated, it might be able to realize sub-ambient cooling even exposed to harsh environmental conditions such as intense solar radiation, humid atmosphere, and small sky-view [6, 7]. RSC has experienced significant advancement in recent years and has demonstrated its applications in PV cooling [8, 9], building energy-saving [10, 11], thermodynamic efficiency improvement [12, 13], water harvesting [14, 15], etc.

However, relatively low cooling power density is one of the main barriers against wider real-world applications of the RSC technology [16, 17]. Regardless of the uncontrollable weather conditions, the cooling capacity of an RSC device can be intrinsically upgraded by dissipating more heat to the sky and absorbing less heat from the environment. Deploying an emitter with desired spectral selectivity, namely, high reflectivity in the solar radiation band and high emissivity in the “atmospheric window”, can significantly enhance the RSC performance [18, 19]. Attributed to the developments in spectrally selective materials, the spectral property of an RSC emitter has been very close to the ideal one, as demonstrated by various emitters

with ultra-high solar reflectivity and long-wave emissivity (e.g., multi-layered [20, 21], nanoparticle-doped [22, 23], and porous [24, 25] structures). However, this also implies that little room is left for further improvement of the cooling performance in this regard. Therefore, other strategies have been identified to further improve the RSC performance, including the introduction of a vacuum scheme to minimize the non-radiative heat exchange between the emitter and ambient [26-28].

Generally, the emitter and the top transparent cover are separated by an air gap in order to suppress the heat exchange between the emitter and ambient air. In typical RSC devices, this air gap is almost at atmospheric pressure. Besides, the backside of the emitter is isolated from the ambient air by a thermal insulation layer, but the emitter and insulator are usually in contact with each other directly. Therefore, vacuumizing the cavity to wipe out the convective and conductive cooling loss of the emitter can improve cooling power density.

To the authors' best knowledge, existing researches about vacuum RSC are mainly experimental studies focusing on pursuing the lowest possible stagnation emitter temperature. No systematic research has been conducted to elucidate the effect of the vacuum mechanism on the RSC performance. Hence, in this study, we conducted a theoretical analysis to comprehensively evaluate the performance of different vacuum-structured RSC modules and to weigh the advantages and disadvantages of involving the vacuum scheme in stand-alone RSC devices. The cooling performance of the RSC module with different vacuum strategies (upper cavity being vacuumized, lower cavity being vacuumized, both cavities being vacuumized, and benchmark case with neither cavity being vacuumized) under different working conditions is investigated.

2. Description of the evacuated RSC module

The cross-section schematic of the four RSC modules, namely, (a) the typical RSC (TRSC) module, (b) the upper-cavity-evacuated RSC (U-ERSC) module, (c) the lower-cavity-evacuated RSC (L-ERSC) module,

and (d) both-cavities-evacuated RSC (UL-ERSC) module, is shown in Fig. 1. The heat exchange between the emitter and its external environment is also shown in Fig.1. The emitter reaches a cooling effect once its outward thermal radiation surpasses the sum of the three parts of incoming heat flow, namely, the absorbed solar radiation, incoming thermal radiation, and non-radiative heat. The transparent cover is a hypothetical hard layer which can stand against the pressure difference between the ambient air and upper cavity and shows a transmissivity of 0.9 throughout 0.2-25 μm . In contrast, the emitter shows distinct spectral selectivity, with an emissivity (absorptivity) of 0.95 in the “atmospheric window” to intensively emit heat to the ambient and an emissivity (absorptivity) of 0.05 in the rest bands to strongly reject heat from the ambient. In addition, a 0.04 m layer of thermal insulator is placed beneath the emitter, with thermal conductivity of 0.033 W/(m·K). The cavity height between the cover and emitter (upper cavity) and that between the emitter and thermal insulator (lower cavity) is 0.03 m. Detailed specifications of the four RSC modules are listed in Table 1.

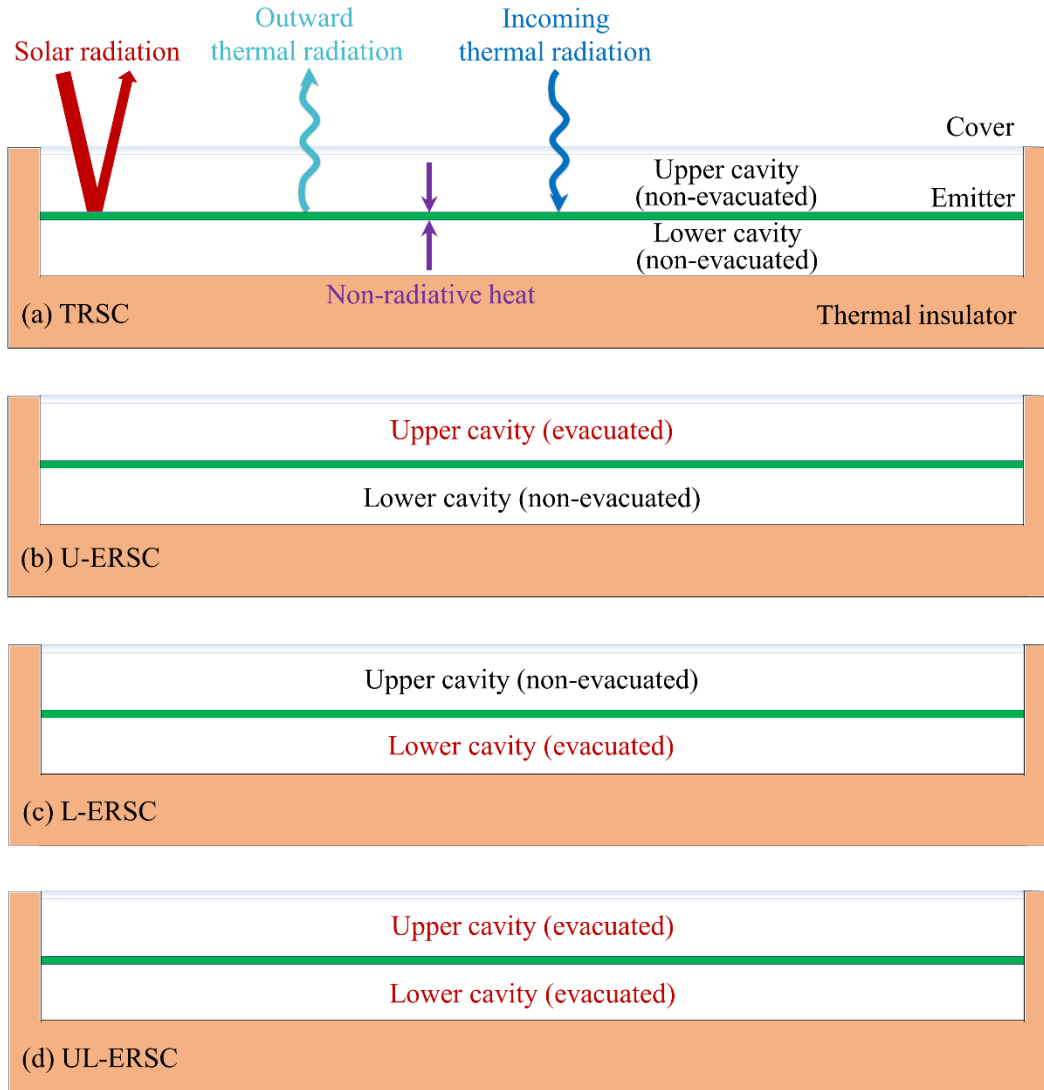


Fig. 1. Schematic of four different RSC modules.

Table 1. Structural parameters of the RSC module.

Components	Parameters	Values
Cover	Length and width	0.5 m
	Emissivity and absorptivity (0.2–25 μm)	0.05
	Transmissivity (0.2–25 μm)	0.9
	Reflectivity (0.2–25 μm)	0.05
Emitter	Emissivity and absorptivity (8–13 μm , upper surface)	0.95
	Emissivity and absorptivity (rest bands, upper surface)	0.05
	Emissivity and absorptivity (0.2–25 μm , lower surface)	0.1
Thermal insulator	Thermal conductivity	0.033 W/(m·K)
	Thickness	0.04 m
Upper cavity	Emissivity and absorptivity (0.2–25 μm , upper surface)	0.1
	Height	0.03 m
Lower cavity	Height	0.03 m
	Thermal conductivity (Wall)	0.022 W/(m·K)

3. Mathematical model

A mathematical model is developed in this section to characterize the cooling performance of the RSC module in different working conditions. The following assumptions are made to simplify the modeling [29]:

- The RSC module operates in the steady- or quasi-steady-state;
- The physical parameters of the cover, emitter, and thermal insulator are constants at different temperatures;
- The temperature of the cover, emitter, and uppermost thermal insulation layer is uniformly distributed along the length and width directions.

The heat-balance equation of the cover is expressed as:

$$h_{ac}(T_a - T_c) + h_{sc}(T_s - T_c) + h_{ec}(T_e - T_c) + \alpha_c G = 0 \quad (1)$$

where h_{ac} is the convective heat transfer coefficient between the cover and ambient air, $W/(m^2 \cdot K)$; h_{sc} is the radiative heat transfer coefficient between the cover and sky, $W/(m^2 \cdot K)$; h_{ec} is the overall heat transfer coefficient between the cover and emitter, $W/(m^2 \cdot K)$; T_a , T_c , T_s , and T_e are respectively the temperature of the ambient air, cover, sky and emitter, K; α_c is the absorptivity of the cover; and G is the solar radiation, W/m^2 .

h_{ac} is calculated by [30]:

$$h_{ac} = 2.8 + 3.0V_a \quad (2)$$

where V_a is the wind velocity, m/s.

h_{sc} is derived by:

$$h_{sc} = \varepsilon_c \sigma (T_s^2 + T_c^2)(T_s + T_c) \quad (3)$$

T_s is expressed as [31]:

$$T_s = 0.0552T_a^{1.5} \quad (4)$$

h_{ec} is calculated by:

$$h_{ec} = h_{ec_conv} + h_{ec_rad} = \frac{Nu \cdot k_a}{d_{ec}} + \frac{\sigma(T_c^2 + T_e^2)(T_c + T_e)}{1/\varepsilon_c - 1/\varepsilon_e - 1} \quad (5)$$

where h_{ec_conv} and h_{ec_rad} are respectively the convective and radiative heat transfer coefficients between the cover and the emitter, $W/(m^2 \cdot K)$; Nu is the Nusselt number; k_a is the thermal conductivity of air in the upper cavity, $W/(m \cdot K)$; d_{ec} is the height of the upper cavity, m; σ is the Stefan–Boltzmann constant, $5.67 \times 10^{-8} W/(m^2 \cdot K^4)$; and ε_c and ε_e are respectively the total, hemispherical emissivity of the cover and emitter.

Nu is expressed as [30]:

$$Nu = \begin{cases} 1 + 1.44 \left(1 - \frac{1708 \cdot (\sin 1.8\varphi)^{1.6}}{Ra \cdot \cos \varphi} \right) \left[1 - \frac{1708}{Ra \cdot \cos \varphi} \right]^+ + \left[\left(\frac{Ra \cdot \cos \varphi}{5830} \right)^{1/3} - 1 \right]^+, & \text{if } T_c < T_e \\ 1 + \left[0.364 \frac{l_e}{d_{ec}} Ra^{1/4} - 1 \right] \sin \varphi, & \text{if } T_c > T_e \\ 0, & \text{if } T_c = T_e \end{cases} \quad (6)$$

where the + exponent signifies that only positive values are used for terms within the square brackets; in the case of negative values, zero is used; φ is the inclination angle of the collector, rad; Ra is the Rayleigh number, and l_e is the length of the emitter, m.

The heat-balance equation of the emitter is expressed as:

$$h_{ec_conv}(T_c - T_e) + h_{ie}(T_i - T_e) + Q_{s_rad} - Q_{e_rad} + (\tau\alpha)_e G = 0 \quad (7)$$

where h_{ie} is the overall heat transfer coefficient between the emitter and thermal insulator, $W/(m^2 \cdot K)$; T_i is the temperature of the thermal insulator, $W/(m^2 \cdot K)$; Q_{s_rad} is the thermal radiation power absorbed by the emitter, W/m^2 ; Q_{e_rad} is the net thermal radiation power dissipated from the emitter to the sky, which involves the radiative heat exchange between the cover and emitter, W/m^2 ; $(\tau\alpha)_e$ is the effective transmissivity–absorptivity product of the emitter.

Similar to the h_{ec} , the h_{ie} is calculated by:

$$h_{ie} = h_{ie_conv} + h_{ie_rad} = \frac{Nu \cdot k_a}{d_{ie}} + \frac{\sigma(T_e^2 + T_i^2)(T_e + T_i)}{1/\varepsilon_e - 1/\varepsilon_i - 1} \quad (8)$$

The Q_{s_rad} is expressed as [32]:

$$Q_{s_rad} = 2 \int_0^\infty \int_0^{\pi/2} \varepsilon_{s,\lambda}(\lambda, \theta) \cdot E_{b,\lambda}(\lambda, T_a) \cdot \alpha_{e,\lambda}(\lambda, \theta) \cdot \tau_{c,\lambda}(\lambda, \theta) \sin \theta \cos \theta d\theta d\lambda \quad (9)$$

where $\varepsilon_{s,\lambda}$, $\alpha_{e,\lambda}$, and $\tau_{c,\lambda}$ are respectively the spectral emissivity of the sky, spectral absorptivity of the emitter, and spectral transmissivity of the cover; $E_{b,\lambda}$ is the spectral radiation power of the blackbody, W/(m²·μm); λ is the wavelength, μm; and θ is the zenith angle, rad.

The Q_{e_rad} is expressed as [32]:

$$Q_{e_rad} = \int_0^\infty \left[\frac{E_{b,\lambda}(T_e) \cdot (1 - \rho_{c,\lambda}) - \varepsilon_{c,\lambda} \cdot E_{b,\lambda}(T_c)}{1/\varepsilon_{e,\lambda} - ((1 - \varepsilon_{e,\lambda})/\varepsilon_{e,\lambda}) \cdot \rho_{c,\lambda}} \right] d\lambda \quad (10)$$

where $\rho_{c,\lambda}$ and $\varepsilon_{c,\lambda}$ are respectively the spectral reflectance and emissivity of the cover; and $\varepsilon_{e,\lambda}$ is the spectral emissivity of the emitter.

The $(\tau\alpha)_e$ is calculated by:

$$(\tau\alpha)_e = \frac{\tau_c \alpha_e}{1 - (1 - \alpha_e) \rho_c} \quad (11)$$

where α_e is the total, hemispherical absorptivity of the emitter; and τ_c and ρ_c are respectively the total, hemispherical transmissivity and reflectance of the cover.

The heat-balance equation of the thermal insulator is expressed as:

$$U_{ai}(T_a - T_i) + h_{ie}(T_e - T_i) = 0 \quad (12)$$

where U_{ai} is the overall heat transfer coefficient between the thermal insulator and ambient air, W/(m²·K), and is derived by:

$$U_{ai} = \frac{1}{1/h_{ai} + d_b/k_b} \quad (13)$$

where h_{ai} is the same as h_{ac} in the formula; and d_b and k_b are respectively the thickness and thermal

conductivity of the thermal insulator, m and $W/(m \cdot K)$.

A computer program using MATLAB was developed based on the above mathematical model to predict the performance of the RSC module. The mathematical model has been experimentally validated in two previous works, one focused on a double-covered daytime solar heating and nighttime radiative cooling module [33], and the other investigated a hybrid photovoltaic–photothermic–radiative cooling collector [34]. The structures of the two prototypes are quite similar to that of the RSC module in this work; therefore, the mathematical model can be used for accurately predicting the thermal performance of the RSC module.

4. Results and discussion

Based on the mathematical model developed in Section 3, a comprehensive numerical study is carried out to evaluate the cooling performance of the four RSC modules. Besides, the effect of some key parameters on the cooling performance of the four modules is characterized as well.

4.1. Stagnation emitter temperatures on a typical summer day

Firstly, the cooling performance of the four RSC modules on a typical summer day is investigated. Shanghai's hourly weather data (ambient temperature, wind velocity, and solar irradiance) on August 17th in the typical meteorological year is derived from the EnergyPlus Weather Data website [35] and employed in this case study, as shown in Fig. 2. The time interval shrinks to 10 seconds by linearly interpolating the hourly data of ambient temperature and solar irradiance in adjacent hours, while the wind velocity is assumed unchanged within each hour.

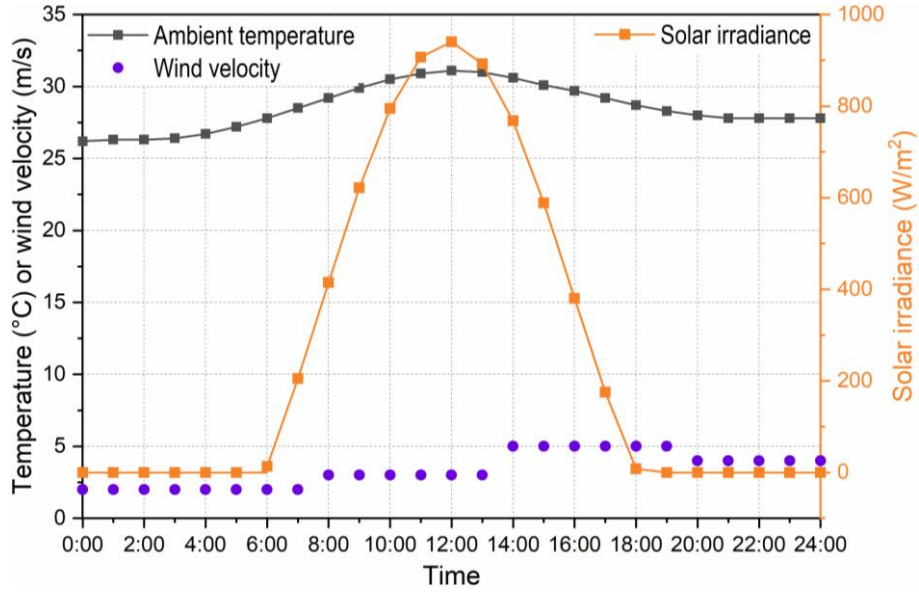


Fig. 2. Hourly ambient temperature, wind velocity, and solar irradiance on August 17th in Shanghai. The data are derived from the typical meteorological year data on the EnergyPlus Weather Data website [35].

As shown in Fig. 3, the four modules can reach sub-ambient temperatures even during peak sun hours, which is mainly contributed by the near-perfect spectral selectivity of the emitter. The vacuum scheme presents a positive effect on lowering the stagnation emitter temperature in this case. The UL-ERSC module shows the lowest stagnation emitter temperature, followed by the U-ERSC and L-ERSC modules, indicating that the upward non-radiative cooling loss of the emitter is greater than the lower one if the cavity is not fully evacuated. Statistically, the maximum temperature gap between the ambient air and emitter is respectively 18.30, 23.79, 20.71, and 28.51 °C at night, while the minimum is correspondingly 4.85, 7.24, 5.32, and 8.24 °C when the solar irradiance exceeds 940 W/m². Hence, the vacuum structure shows much greater performance enhancement during the nighttime than in the daytime. For instance, vacuumization in both cavities enables a further temperature reduction of 10.21 °C during the nighttime, but this value remarkably decreases to only 3.39 °C during the daytime.

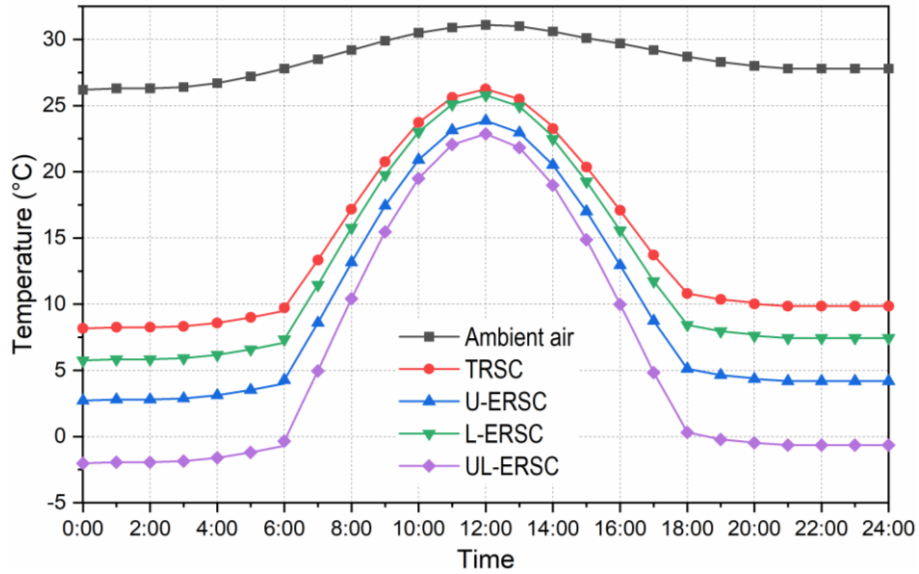


Fig. 3. Stagnation emitter temperatures of the four different RSC modules with the emissivity of the emitter being 0.95 in the “atmospheric window” and 0.05 excluding this spectral range.

However, the vacuum scheme will not always facilitate heat dissipation from the emitter, supposing the spectral selectivity of the emitter is not as favorable as the settings in Table 1. In this case, the vacuum strategy may negatively affect the cooling performance of the RSC module. For example, Fig. 4 illustrates the stagnation emitter temperature profile of the four RSC modules with the emissivity of the emitter being 0.9 in the “atmospheric window” and 0.1 excluding this range (a spectral selectivity not as good as the 0.95-0.05 one but also very close to the ideal case). It is clear that none of the four RSC modules can realize an all-day sub-ambient cooling effect in this case. When the emitter temperature is lower than the ambient temperature, the vacuumization can still minimize the non-radiative heat transferred from nearby warm bodies to the emitter. However, when the emitter temperature exceeds the ambient temperature in peak sun hours (roughly from 9:04 to 14:40), the vacuum scheme will suppress the non-radiative heat transferred from the emitter to the surroundings. Specifically, at 12:00, vacuum in the upper cavity, lower cavity, and both cavities result in a stagnation emitter temperature increment of 1.69, 0.34, and 2.39 °C, respectively.

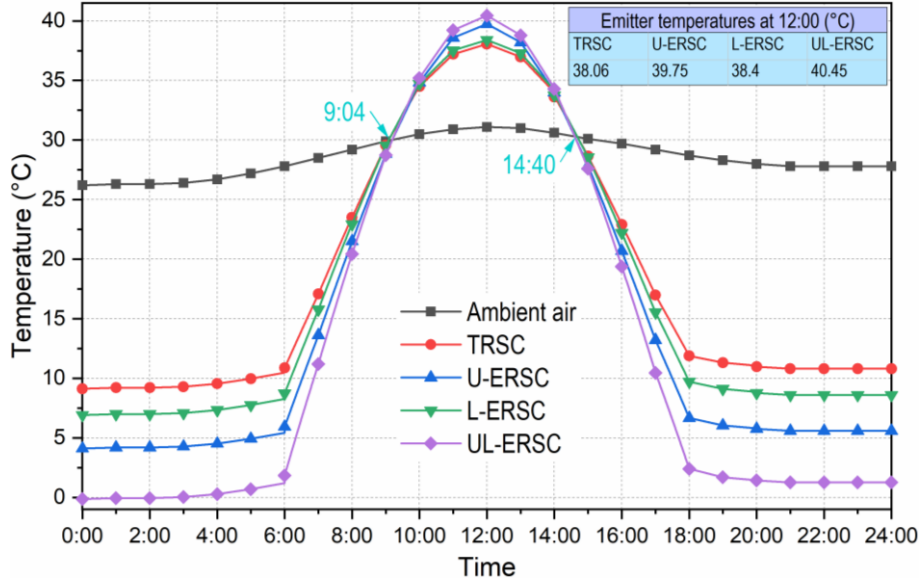


Fig. 4. Stagnation emitter temperatures of the four different RSC modules with the emissivity of the emitter being 0.9 in the “atmospheric window” and 0.1 excluding this range.

Although advancements in materials science have made the delivery of a near-ideal RSC emitter accessible, the emitter may still be unable to realize daytime sub-ambient cooling in the real world due to harsh weather conditions such as intense solar radiation and high relative humidity [36]. In such scenarios, the vacuum scheme will deteriorate rather than ameliorate the cooling performance of an RSC device.

4.2. Cooling power at different emitter temperatures

Compared to the stagnation temperature, the cooling power available from the emitter is a more practical indicator for the performance characterization of an RSC device. Therefore, the cooling power of the four RSC modules at different emitter temperatures is evaluated and compared in this section. The ambient temperature, wind velocity, and solar irradiance are set at 30 °C, 2 m/s, and 0 W/m², respectively. Eq. (7) is accordingly adjusted as follows:

$$h_{ec_conv} (T_c - T_e) + h_{ie} (T_i - T_e) + Q_{s_rad} - Q_{e_rad} + (\tau\alpha)_e G - Q_{cooling} = 0 \quad (14)$$

where $Q_{cooling}$ refers to the cooling power output of the emitter, W/m².

As shown in Fig. 5, when the emitter temperature equals the ambient temperature, the four modules have almost the same cooling power, around 64.5 W/m^2 . As the emitter temperature declines, the thermal radiant power of the emitter degrades and the non-radiative cooling loss upgrades, resulting in a gradual decrement in the cooling capacity for all four modules. However, attributed to the vacuum scheme, the decrements of the three vacuum-based RSC modules are slower than the typical one. When the emitters in the four modules reach their stagnation temperatures (11.33 , 8.93 , 5.78 , and $1.01 \text{ }^\circ\text{C}$, respectively in this case), the cooling power reduces to zero. The benefit contributed by the vacuumization enlarges as the emitter approaches its stagnation temperature, which is well-demonstrated in Figs. 5 and 6. However, in actual working conditions, the emitter will be warmed by a hot working medium such as water and air and thus unable to reach a temperature far below the ambient temperature. Generally, a nighttime temperature difference of $5 \text{ }^\circ\text{C}$ between the emitter and ambient air is reasonable and common in real-world dynamic operations with the involvement of a thermal carrier (this value will be even smaller in the daytime). Under this premise, the cooling power enhancement resulting from the vacuum scheme is limited. Compared to the TRSC module, the relative cooling power improvement of the U-ERSC, L-ERSC, and UL-ERSC modules is respectively 7.58% , 3.32% , and 10.90% , corresponding to only 3.54 , 1.55 , and 5.10 W/m^2 extra cooling gains. With an eye to the addition of energy consumption and system complexity caused by the vacuum unit, it may not be advisable to pursue better RSC performance with the vacuum strategy, unless realizing a deep stagnation emitter temperature is targeted.

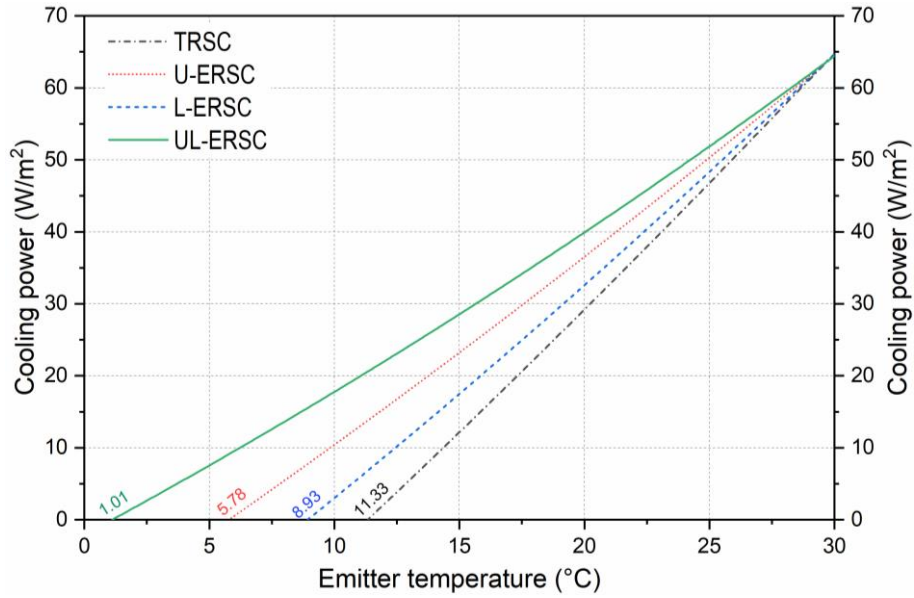


Fig. 5. Cooling power of the four RSC modules at different emitter temperatures. The ambient temperature, wind velocity, and solar irradiance are set at 30 °C, 2 m/s, and 0 W/m², respectively.

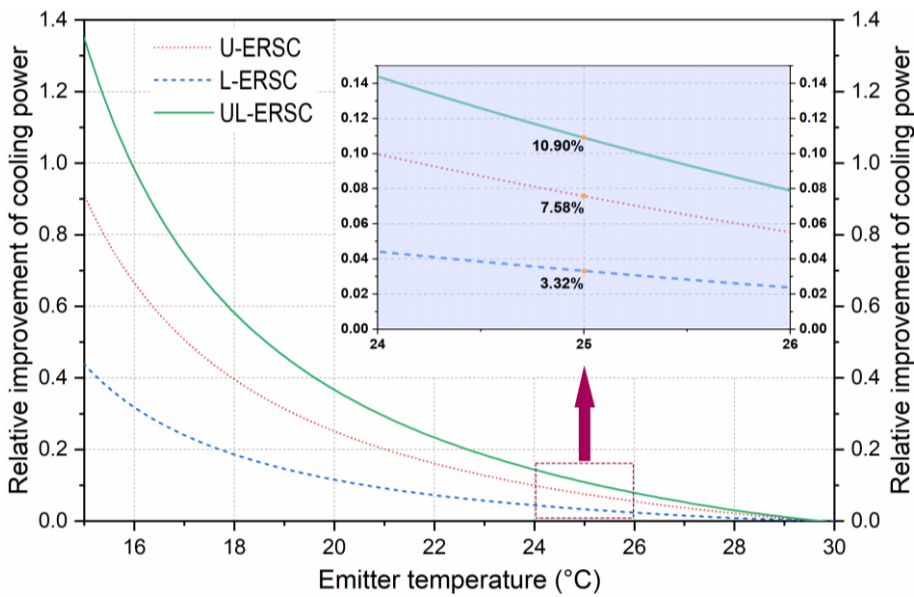


Fig. 6. Relative cooling power improvement of the three evacuated RSC modules at different emitter temperatures. The ambient temperature, wind velocity, and solar irradiance are set at 30 °C, 2 m/s, and 0 W/m², respectively.

4.3. Coupling effect of emitter temperatures and vacuum degrees

In real-world applications, the discussed air cavities in the RSC modules can barely realize a perfect vacuum state, and the vacuum degree would gradually decrease after long-term operation. This would further

lower the contribution of the vacuum scheme to cooling performance enhancement. Therefore, in this section, the effect of vacuum degrees on the performance of the three evacuated RSC modules at different emitter temperatures is investigated. The ambient temperature, wind velocity, and solar irradiance are set at 30 °C, 2 m/s, and 0 W/m², respectively. Here a parameter named as “vacuum factor (φ)” is used to represent the vacuum degree of the discussed cavities, which affects the non-radiative heat transfer coefficient in the cavity. When the vacuum factor is 0, the non-radiative heat transfer coefficient reaches zero and thus the cavity is fully evacuated; when the vacuum factor is 1, the non-radiative heat transfer coefficient equals that in the air cavity of the TRSC module and thus no vacuum scheme is involved.

Fig. 7 illustrates the cooling power contour of the three evacuated RSC modules against different emitter temperatures and vacuum factors. As the emitter temperature decreases, the temperature gap between the air in the cavities and ambient enlarges and thus the vacuum factor exerts an increasing effect on the cooling performance of the three evacuated modules. Moreover, As the vacuum factor increases, the cooling power declines nearly linearly for the U-ERSC module but drops with decreased rates for the L-ERSC and UL-ERSC modules. The cooling performance of the L-ERSC module is least sensitive while that of the UL-ERSC module is most sensitive to the vacuum factor. For instance, as the vacuum degree increases from 0 to 0.5, the stagnation emitter temperature of the L-ERSC module slightly elevates from 8.93 to 10.87 °C while that of the UL-ERSC module remarkably increases from 1.01 to 8.46 °C. Lastly, it is clear that the UL-ERSC module shows the minimum non-cooling zone, indicating that it has the best cooling performance among the three.

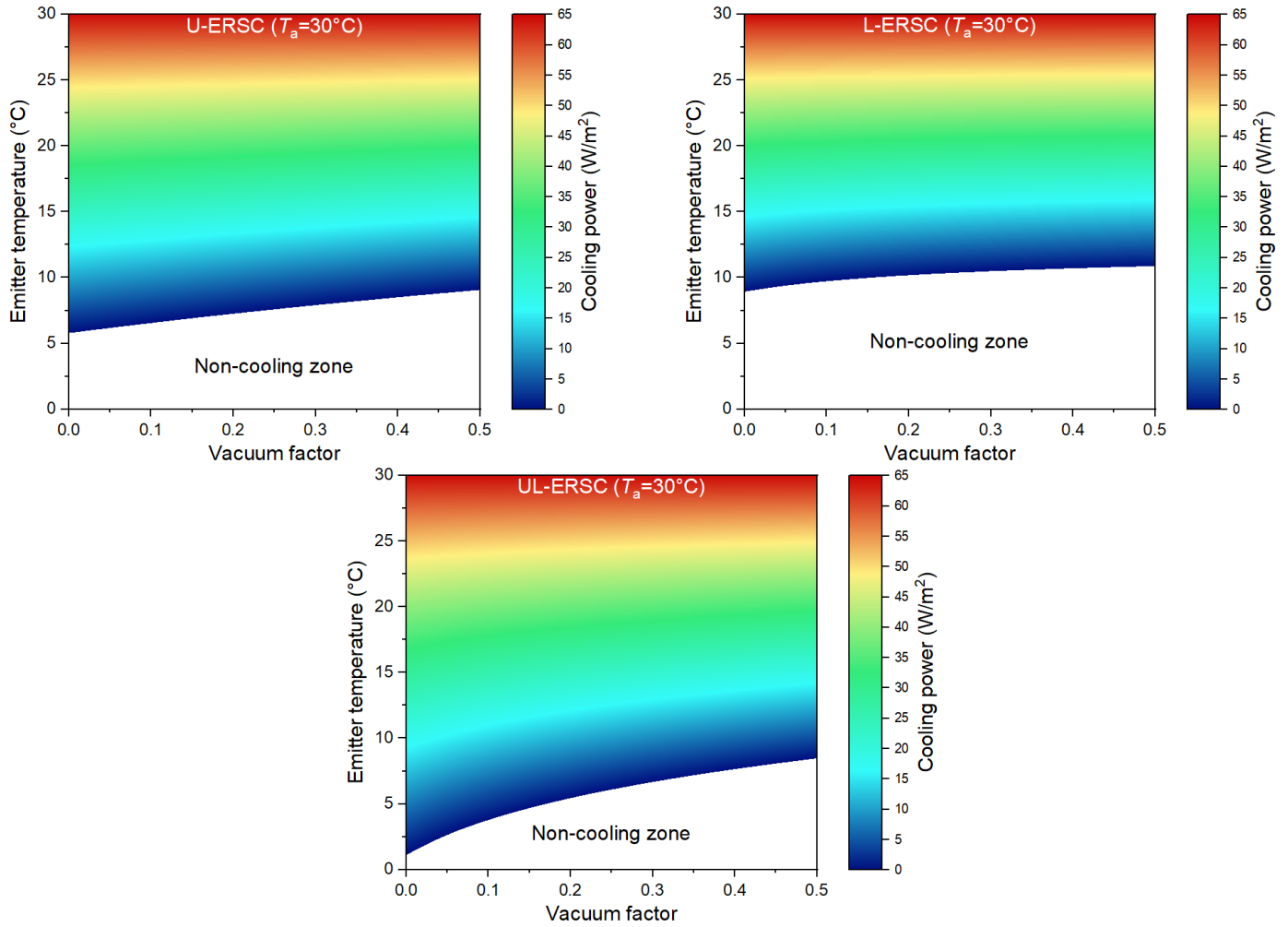


Fig. 7. Coupling effect of emitter temperatures and vacuum factors on the cooling performance of the three evacuated RSC modules. The ambient temperature, wind velocity, and solar irradiance are set at 30 °C, 2 m/s, and 0 W/m², respectively.

As previously stated, a thermal carrier passing beneath the emitter will extract cooling energy from the emitter and thus warm it in real working conditions. Hence, a reasonable ambient-emitter temperature gap of 5 °C is assumed to reveal the relative cooling power improvement of the three evacuated RSC modules with different vacuum degrees compared to the TRSC module. As shown in Fig. 8, all three evacuated RSC modules show decreased relative cooling power improvements as the vacuum factor increases. The UL-ERSC module presents the greatest improvement in all cases, followed by the U-ERSC module. As the backside thermal insulation layer already significantly suppresses the heat exchange between the emitter and ambient air, the contribution from the evacuated lower cavity is thus limited and the L-ERSC module shows much

lower relative cooling power improvements at different vacuum factors compared to the U-ERSC module, with the value being only 0.84% when the vacuum factor reaches 0.5.

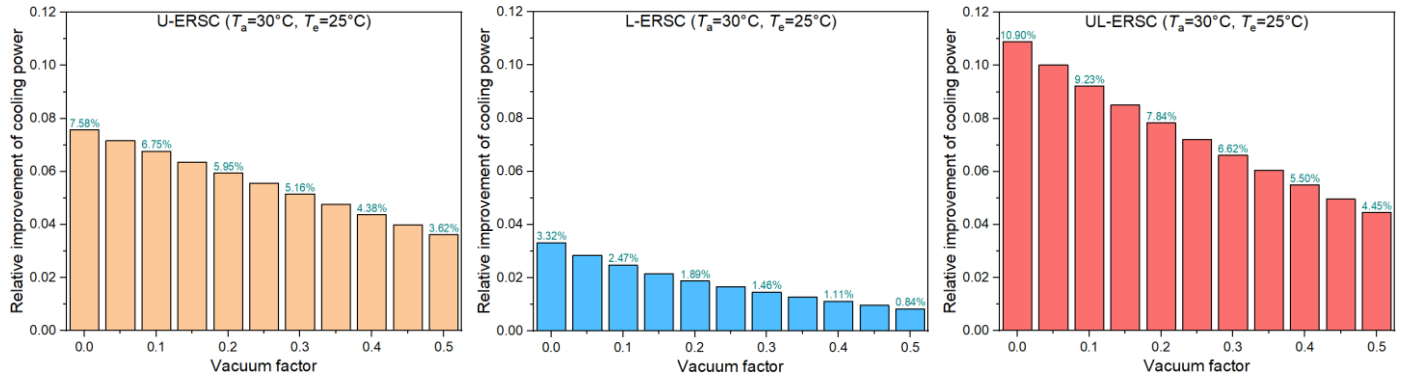


Fig. 8. Relative cooling power improvement of the three evacuated RSC modules at different vacuum factors with an emitter temperature of 25 °C. The ambient temperature, wind velocity, and solar irradiance are set at 30 °C, 2 m/s, and 0 W/m², respectively.

However, the situation might be reversed if the backside thermal insulation thickness changes. As shown in Fig. 9, the contribution from the evacuated lower cavity magnifies gradually at decreased insulation thickness. In the present study, the standard thickness of the thermal insulation layer is 4 cm. However, if the thickness is less than 1.2 cm, the relative cooling power improvement contributed by the evacuated lower cavity exceeds that caused by the evacuated upper cavity, giving a vacuum factor of 0.1. Assuming an extreme case in which the thickness of the backside thermal insulation layer is 0 (considering that no thermal insulation is on top of the cover as well), the relative cooling power improvement of the L-ERSC module reaches 17.19%, which is much higher than that of the U-ERSC module (7.89%). For the upper cavity, as the emitter is a cold bottom surface, the non-radiative heat transfer from the top to the bottom surface is exclusively by conduction ($Nu=1$) [37]. For the lower cavity, however, as the emitter is a cold top surface, the non-radiative heat transfer from the bottom to the top surface involves both conduction and free convection, thus the vacuum scheme will suppress the heat transfer more effectively. Nevertheless, the backside thermal insulation layer can be easily and cheaply arranged with a sufficient thickness to fully replace the vacuum to thermally isolate the

emitter from warm ambient air. Fig. 10 shows the cooling power of the TRSC module at different thermal insulator thicknesses. It is clear that, with an insulator thicker than 8.3 cm, its cooling power will exceed that of the L-ERSC module with an insulator thickness of 4 cm and a vacuum factor of 0.1, and this critical insulator thickness will be smaller if the vacuum factor of the L-ERSC module is greater than 0.1. This further suggests that getting a higher cooling capacity with a vacuum scheme is unnecessary, at least for the lower cavity. For the upper cavity, a hard cover with enough mechanical strength is essential to withstand the pressure difference between the upper cavity and the environment. Therefore, the most common cover material, namely, polyethylene film, is not suitable for vacuum RSC devices. Other cover materials such as zinc sulfide, kalium chloratum, and diamond are robust enough but face challenges such as relatively low long-wave transmissivity, easy deliquescence, and high cost. Therefore, the unavailability of desired covers is another challenge for high-performance and practical radiative cooling using the vacuum scheme.

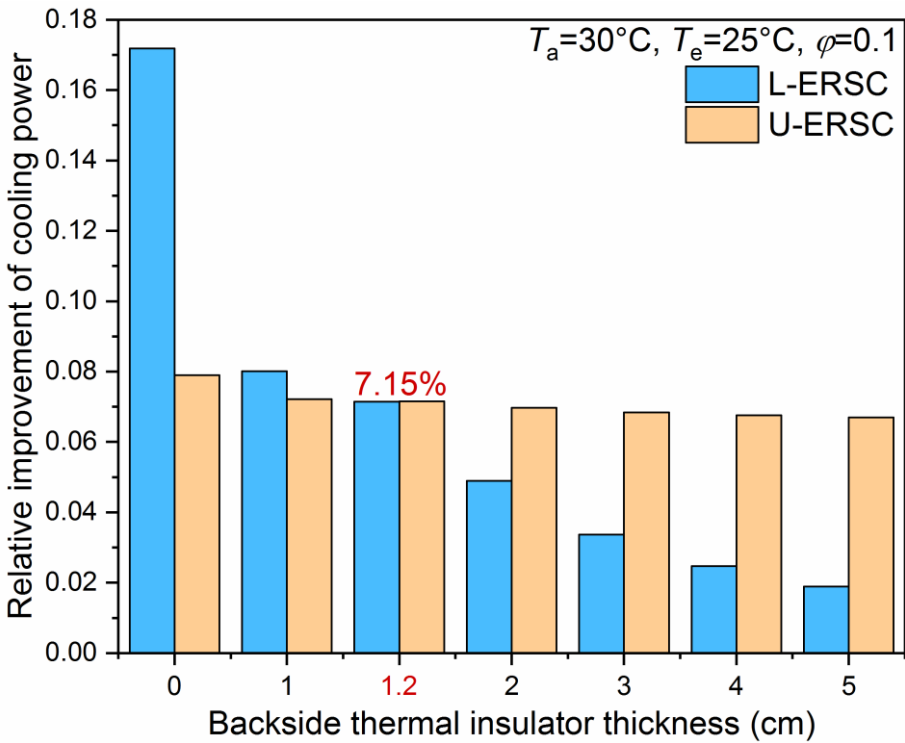


Fig. 9. Relative cooling power improvement of the L-ERSC module at different backside thermal insulator thicknesses with an emitter temperature of 25 °C and a vacuum factor of 0.1. The ambient temperature, wind velocity, and solar irradiance are set at 30 °C, 2 m/s, and 0 W/m², respectively.

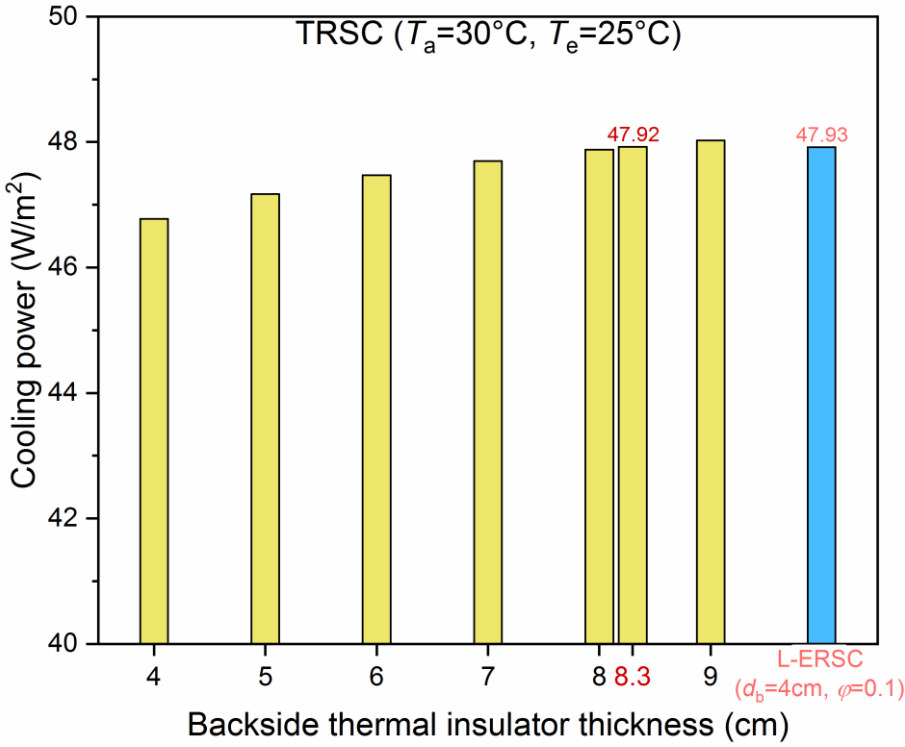


Fig. 10. Cooling power of the TRSC module at different backside thermal insulator thicknesses with an emitter temperature of 25 °C. The ambient temperature, wind velocity, and solar irradiance are set at 30 °C, 2 m/s, and 0 W/m², respectively.

5. Conclusions

In the present study, a radiative sky cooling (RSC) module with four vacuum structures is proposed to evaluate the performance improvement contributed by the vacuum scheme. A quasi-steady state mathematical model is developed to characterize the cooling performance of the four RSC modules under different operation conditions. The detailed results are summarized as follows:

- (1) If the typical RSC (TRSC) module itself can realize all-day sub-ambient cooling, the vacuum strategy can further elevate the cooling capacity. The both-cavities-evacuated RSC (UL-ERSC) module shows the best cooling performance among the four, followed by the upper-cavity-evacuated RSC (U-ERSC)

module and the lower-cavity-evacuated RSC (L-ERSC) module. However, if the TRSC cannot achieve sub-ambient cooling during peak sun hours, the vacuum scheme will deteriorate rather than ameliorate the cooling performance. This is very likely to occur in practice, especially under harsh weather conditions.

- (2) On a typical summer day in Shanghai, vacuumization in both cavities enables a further temperature reduction of 10.21 °C during the nighttime, but this value can decrease to only 3.39 °C during the daytime.
- (3) The cooling power enhancement resulting from the vacuum scheme is limited in real-world dynamic operation with the thermal carrier. At a reasonable temperature gap of 5 °C between the emitter and ambient air, the extra cooling gain is less than 5.10 W/m².
- (4) The cooling performance enhancement benefiting from the vacuum scheme in the lower cavity can be well replaced by a sufficiently thick thermal insulation layer beneath the emitter, while developing a high-performance, low-cost, and mechanically robust cover for forming the evacuated upper cavity is still a challenge.
- (5) Considering the addition of energy consumption and system complexity caused by the vacuum unit, it may not be advisable to pursue higher cooling performance of a stand-alone RSC collector/system through introducing a vacuum strategy, unless realizing a deep stagnation emitter temperature is targeted.

Acknowledgments

This study was sponsored by the National Natural Science Foundation of China (NSFC 51906241, 51776193, and 52106276), H2020 Marie Skłodowska-Curie Actions - Individual Fellowships (842096), and Anhui Provincial Natural Science Foundation (1908085ME138 and 2008085QE234).

Nomenclature

d Thickness, m

E	Spectral radiation power of the blackbody, $W/(m^2 \cdot \mu m)$
G	Solar energy, W/m^2
h	Heat transfer coefficient, $W/(m^2 \cdot K)$
k	Thermal conductivity, $W/(m \cdot K)$
l	Length, m
Nu	Nusselt number, -
Q	Thermal radiation power, W/m^2
Ra	Rayleigh number, -
T	Temperature, K
U	Overall heat transfer coefficient, $W/(m^2 \cdot K)$
V	Wind velocity, m/s
α	Absorptivity, -
β	Inclination angle, rad
τ	Transmissivity, -
$(\tau\alpha)$	Effective transmissivity–absorptivity product, -
ε	Emissivity, -
ρ	Reflectivity, -
σ	Stefan–Boltzmann constant, $5.67 \times 10^{-8} W/(m^2 \cdot K^4)$
θ	Zenith angle, rad
λ	Wavelength, μm
φ	Vacuum factor, -

Abbreviation and subscripts

a	Ambient air
c	Cover
conv	Convection
cooling	Cooling power
e	Emitter
i	Thermal insulator
rad	Radiation
s	Sky

References

[1] D. Zhao, A. Aili, Y. Zhai, S. Xu, G. Tan, X. Yin, R. Yang, Radiative sky cooling: Fundamental principles, materials, and applications, *Applied Physics Reviews*, 6 (2019).

- [2] L. Chen, K. Zhang, M. Ma, S. Tang, F. Li, X. Niu, Sub-ambient radiative cooling and its application in buildings, *Building Simulation*, (2020).
- [3] M. Hu, B. Zhao, X. Ao, J. Cao, Q. Wang, S. Riffat, Y. Su, G. Pei, Applications of radiative sky cooling in solar energy systems: Progress, challenges, and prospects, *Renewable and Sustainable Energy Reviews*, 160 (2022) 112304.
- [4] J. Zhang, Z. Zhou, H. Tang, J. Xing, J. Quan, J. Liu, J. Yu, M. Hu, Mechanically Robust and Spectrally Selective Convection Shield for Daytime Subambient Radiative Cooling, *ACS Appl Mater Interfaces*, 13 (2021) 14132-14140.
- [5] D. Xu, S. Boncoeur, G. Tan, J. Xu, H. Qian, D. Zhao, Energy saving potential of a fresh air pre-cooling system using radiative sky cooling, in: *Building Simulation*, Vol. 15, Springer, 2022, pp. 167-178.
- [6] A. Leroy, B. Bhatia, C.C. Kelsall, A. Castillejo-Cuberos, M. Di Capua H., L. Zhao, L. Zhang, A.M. Guzman, E.N. Wang, High-performance subambient radiative cooling enabled by optically selective and thermally insulating polyethylene aerogel, *Science Advances*, 5 (2019) eaat9480.
- [7] H. Zhong, P. Zhang, Y. Li, X. Yang, Y. Zhao, Z. Wang, Highly solar-reflective structures for daytime radiative cooling under high humidity, *ACS Applied Materials & Interfaces*, 12 (2020) 51409-51417.
- [8] B. Zhao, M. Hu, X. Ao, Q. Xuan, G. Pei, Spectrally selective approaches for passive cooling of solar cells: A review, *Applied Energy*, 262 (2020) 114548.
- [9] K. Wang, G. Luo, X. Guo, S. Li, Z. Liu, C. Yang, Radiative cooling of commercial silicon solar cells using a pyramid-textured PDMS film, *Solar Energy*, 225 (2021) 245-251.
- [10] Z. Yi, D. Xu, J. Xu, H. Qian, D. Zhao, R. Yang, Energy saving analysis of a transparent radiative cooling film for buildings with roof glazing, *Energy and Built Environment*, 2 (2021) 214-222.
- [11] D. Shen, C. Yu, W. Wang, Investigation on the thermal performance of the novel phase change materials wall with radiative cooling, *Applied Thermal Engineering*, 176 (2020) 115479.
- [12] W. Li, S. Buddhiraju, S. Fan, Thermodynamic limits for simultaneous energy harvesting from the hot sun and cold outer space, *Light: Science & Applications*, 9 (2020) 68.
- [13] M. Zeyghami, F. Khalili, Performance improvement of dry cooled advanced concentrating solar power plants using daytime radiative cooling, *Energy Conversion and Management*, 106 (2015) 10-20.
- [14] J. Xu, J. Zhang, B. Fu, C. Song, W. Shang, P. Tao, T. Deng, All-Day Freshwater Harvesting through Combined Solar-Driven Interfacial Desalination and Passive Radiative Cooling, *ACS Applied Materials & Interfaces*, 12 (2020) 47612-47622.
- [15] C. Liu, J. Fan, H. Bao, Hydrophilic radiative cooler for direct water condensation in humid weather, *Solar Energy Materials and Solar Cells*, 216 (2020) 110700.
- [16] U. Eicker, A. Dalibard, Photovoltaic-thermal collectors for night radiative cooling of buildings, *Solar Energy*, 85 (2011) 1322-1335.
- [17] S. Ahmed, Z. Li, T. Ma, M.S. Javed, H. Yang, A comparative performance evaluation and sensitivity analysis of a photovoltaic-thermal system with radiative cooling, *Solar Energy Materials and Solar Cells*, 221 (2021) 110861.
- [18] J. Fan, C. Fu, T. Fu, Yttria-stabilized zirconia coating for passive daytime radiative cooling in humid environment, *Applied Thermal Engineering*, 165 (2020) 114585.
- [19] Z. Cheng, Y. Shuai, D. Gong, F. Wang, H. Liang, G. Li, Optical properties and cooling performance analyses of single-layer radiative cooling coating with mixture of TiO₂ particles and SiO₂ particles, *Science China Technological Sciences*, 64 (2021) 1017-1029.
- [20] A.P. Raman, M.A. Anoma, L. Zhu, E. Rephaeli, S. Fan, Passive radiative cooling below ambient air temperature under direct sunlight, *Nature*, 515 (2014) 540-544.
- [21] D. Chae, M. Kim, P.-H. Jung, S. Son, J. Seo, Y. Liu, B.J. Lee, H. Lee, Spectrally selective inorganic-based multilayer emitter for daytime radiative cooling, *ACS Applied Materials & Interfaces*, 12 (2020) 8073-8081.
- [22] Z. Cheng, H. Han, F. Wang, Y. Yan, X. Shi, H. Liang, X. Zhang, Y. Shuai, Efficient radiative cooling coating with biomimetic human skin wrinkle structure, *Nano Energy*, 89 (2021) 106377.

- [23] D. Chae, H. Lim, S. So, S. Son, S. Ju, W. Kim, J. Rho, H. Lee, Spectrally selective nanoparticle mixture coating for passive daytime radiative cooling, *ACS Applied Materials & Interfaces*, 13 (2021) 21119-21126.
- [24] H.-D. Wang, C.-H. Xue, X.-J. Guo, B.-Y. Liu, Z.-Y. Ji, M.-C. Huang, S.-T. Jia, Superhydrophobic porous film for daytime radiative cooling, *Applied Materials Today*, 24 (2021) 101100.
- [25] S. Son, Y. Liu, D. Chae, H. Lee, Cross-linked porous polymeric coating without a metal-reflective layer for sub-ambient radiative cooling, *ACS Applied Materials & Interfaces*, 12 (2020) 57832-57839.
- [26] Z. Chen, L. Zhu, A. Raman, S. Fan, Radiative cooling to deep sub-freezing temperatures through a 24-h day-night cycle, *Nat Commun*, 7 (2016) 13729.
- [27] Z. Chen, L. Zhu, W. Li, S. Fan, Simultaneously and Synergistically Harvest Energy from the Sun and Outer Space, *Joule*, 3 (2019) 101-110.
- [28] C.Y. Tso, K.C. Chan, C.Y.H. Chao, A field investigation of passive radiative cooling under Hong Kong's climate, *Renewable Energy*, 106 (2017) 52-61.
- [29] M. Hu, B. Zhao, X. Ao, Y. Su, Y. Wang, G. Pei, Comparative analysis of different surfaces for integrated solar heating and radiative cooling: A numerical study, *Energy*, 155 (2018) 360-369.
- [30] C. Guo, J. Ji, W. Sun, J. Ma, W. He, Y. Wang, Numerical simulation and experimental validation of tri-functional photovoltaic/thermal solar collector, *Energy*, 87 (2015) 470-480.
- [31] J.A. Duffie, W.A. Beckman, *Solar engineering of thermal processes*, John Wiley & Sons, 2013.
- [32] M. Hu, Suhendri, B. Zhao, X. Ao, J. Cao, Q. Wang, S. Riffat, Y. Su, G. Pei, Effect of the spectrally selective features of the cover and emitter combination on radiative cooling performance, *Energy and Built Environment*, 2 (2021) 251-259.
- [33] M. Hu, B. Zhao, X. Ao, N. Chen, J. Cao, Q. Wang, Y. Su, G. Pei, Feasibility research on a double-covered hybrid photo-thermal and radiative sky cooling module, *Solar Energy*, 197 (2020) 332-343.
- [34] M. Hu, B. Zhao, X. Ao, X. Ren, J. Cao, Q. Wang, Y. Su, G. Pei, Performance assessment of a trifunctional system integrating solar PV, solar thermal, and radiative sky cooling, *Applied Energy*, 260 (2020) 114167.
- [35] EnergyPlus Weather Data (<https://energyplus.net/weather>).
- [36] B. Zhao, M. Hu, X. Ao, G. Pei, Performance evaluation of daytime radiative cooling under different clear sky conditions, *Applied Thermal Engineering*, 155 (2019) 660-666.
- [37] T.L. Bergman, F.P. Incropera, D.P. DeWitt, A.S. Lavine, *Fundamentals of heat and mass transfer*, John Wiley & Sons, 2011.